Article

Activated Carbon Prepared from Waste Coffee Grounds: Characterization and Adsorption Properties of Dyes

Ferielle Aouay , Attia Afef , Lasaad Damak , Raja Ben Amar * , Andre Deratani *

Posted Date: 14 May 2024

doi: 10.20944/preprints202405.0964.v1

Keywords: dye removal; AO7; activated carbon; spent coffee grounds; adsorption process; experimental design methodology; optimization

doi:10.20944/preprints202405.0964.v1

Article

Activated Carbon Prepared from Waste Coffee Grounds: Characterization and Adsorption Properties of Dyes

Feryelle Aouay [1,2], Afef Attia [1], Lasaad Dammak [3], Raja Ben Amar [1,*] and Andre Deratani [2,*]

[1] Research Unit "Advanced Technologies for Environment and Smart Cities", Faculty of Sciences, University of Sfax, 3000 Sfax, Tunisia
[2] Institut Europeen des Membranes, IEM, UMR-5635, ENSCM, CNRS, University Montpellier, 34095 Montpellier, France
[3] Université Paris Est Creteil, CNRS, ICPME, UMR 7182, 2 rue Henri Dunant, 94320 Thiais, France
* Correspondence: raja.benamar@fss.usf.tn (R.B); andre.deratani@umontpellier.fr (A.D.)

Abstract: Spent coffee grounds (SCG) have great potential as a useful, value-added biological material. In this context, activated carbon (AC) was prepared from SCG by an activation process using H_3PO_4 at 600°C in air and used as an adsorbent for the azo dye AO7, a model molecule for dye colorants found in textile industry effluents. X-ray diffraction, SEM and BET revealed that the AC was predominantly amorphous, consisting of a powder of 20-100 μm particles with mesopores averaging 5.5 nm in pore size. Adsorption kinetics followed a pseudo-second-order law, while the Langmuir model best fitted experimental isotherm data (maximum capacity of 119.5 mg AO7 per AC g). Thermodynamic parameters revealed that adsorption was endothermic and spontaneous. All the characterizations indicated that adsorption occurred by physisorption via mainly π-π interactions. The best experimental removal efficiency optimized by means of a Box-Behnken design and response surface methodology was 98% for an initial AO7 concentration of 20 $mg.L^{-1}$ at pH 7.5 with a dose of 0.285 $g.L^{-1}$ of AC and a contact time of 40 min. These results clearly show that activated carbon prepared from SCG can be a useful material for efficiently removing organic matter from aqueous solutions.

Keywords: dye removal; AO7; activated carbon; spent coffee grounds; adsorption process; experimental design methodology; optimization

---

1. Introduction

Water is an essential resource whose integrity is often compromised by the discharge of industrial waste containing harmful substances into natural environments [1]. A striking example of this challenge is the treatment of contaminated industrial wastewater, particularly from the textile industry, one of the biggest water consumers [2]. This industry generates a large volume of waste loaded with dyes and chemicals, posing a threat to human health and the environment [3]. Synthetic dyes, especially azo dyes, are of particular concern because of their carcinogenic, mutagenic and teratogenic properties, as well as the high chemical and biological oxygen demand required for their degradation [4,5]. Acid Orange 7 (AO7), an azo dye widely used as a model molecule, exemplifies these challenges. Despite its water-solubility and stability, AO7 can cause methemoglobinemia upon human exposure, resulting in symptoms such as cyanosis and weakness [5–7].

Azo dyes, characterized by an azo chromophore group (-N=N-) and an electron-receiving sulfonate group ($-SO3^{-}$), are difficult to degrade by conventional processing methods [8–10]. In fact, textile dyes are not easily biodegradable, requiring the development of specific microbial strains and immobilized enzymes. [11]. Another approach to decontaminating water polluted by textile dyes is the use of physico-chemical techniques, including electrochemical oxidation [12], coagulation-flocculation [13], filtration [14,15] and photodegradation [16]. However, these methods often have drawbacks such as high costs and the production of toxic by-products. Adsorption appears to be a promising alternative approach due to its cost-effectiveness and its ability to remove contaminants without introducing additional toxicity [17,18]. Activated carbon (AC) is emerging as an adsorbent of choice, especially when derived from natural biopolymers or waste products, offering a sustainable and cost-effective solution for water purification [8]. The production of AC from inexpensive feedstocks available in large quantities makes it possible to envisage an easily scalable adsorption process [19]. In this work, spent coffee grounds (SCGs) were chosen as a precursor to produce AC [20,21].

Coffee is one of the world's most popular beverages. Every year, more than five million tons of coffee are produced worldwide (International Coffee Organization, 2022). Generally, SCGs are disposed of by composting, incineration or landfill. It has been reported that these methods can have a negative impact on the environment, releasing contaminating residues of tannin, caffeine and polyphenols [22]. Other ways of valorizing SCGs has been proposed, such as converting them into biofuel, biodiesel, bioethanol, or biomaterials [23] and producing biochar and AC [24–26]. These routes can help reinforce the circular economy approach by enabling continuous processes that reduce the accumulation of waste by transforming it into useful, value-added materials while promoting more environmentally friendly models [27,28].

This study examined the removal of AO7, as a model molecule for azo-dye used in textile industry, by adsorption onto AC produced from SCGs. The physico-chemical properties of the AC produced were investigated using techniques such as TGA-DTG, XRD, FT-IR and SEM. With a view to optimizing the process, studies including adsorption kinetics and isotherms as well as thermodynamic characteristics were carried out to understand how certain experimental parameters such as dye concentration/adsorbent quantity ratio and contact time can affect the adsorption operation. A statistical analysis was then applied to assess the weight of each of the experimental parameters. The Response Surface Methodology (RSM) model was used to analyze the interactions among the parameters studied in order to gain a better insight into their combined effects. This method has the advantage of evaluating several parameters at once, which reduces the number of experiments required and saves time compared with the traditional method of examining one factor at a time [29,30]. In addition, the efficiency of experimental systems can be effectively evaluated, and process variability minimized.

2. Materials and Methods

2.1. Chemicals

The SCG used in the present study was collected from local coffee shops and served as a low-cost precursor for AC. Phosphoric acid (H_3PO_4, 50%) was used as a chemical activating agent in the preparation of AC. The azo dye AO7 (analytical grade ≥ 85%), whose characteristics are given in Table 1, was supplied by Sigma-Aldrich (Saint Louis, MO, USA). All aqueous solutions were prepared with deionized water and pH adjusted with sodium hydroxide (NaOH, 0.2M) and hydrochloric acid (HCl, 0.2M).

Table 1. Main characteristics of AO7.

Chemical structure	**Molecular formula**	**Molecular weight (g.mol^{-1})**	**Solubility in water (g.L^{-1})**	**Melting point (°C)**	**⚜max (nm)**
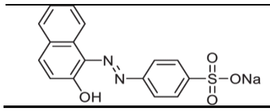	$C_{16}H_{11}N_2SO_4Na$	350.32	116	164	483

doi:10.20944/preprints202405.0964.v1

2.2. Activated Carbon Preparation

The following procedure, adapted from [31], was applied for the preparation of SCG-based AC. Typically, SCG (30 g) was washed with deionized water, then dried in an oven at 60°C. The resulting dried SCG was immersed in a 50% solution of H3PO4 in a weight ratio of 1:3 (SCG:H3PO4) and stirred at 80°C for 3 hours. Slow pyrolysis was then carried out at 600°C for 2 hours in a muffle furnace in air. The resulting AC was washed with deionized water to neutral pH, and then finally dried in an electric oven at 105°C for 24 hours.

2.3. Characterization of AC

The produced AC was characterized using FTIR (Spectrum 100, Perkin Elmer, USA) and SEM (Quanta-250, Thermo Fisher Scientific, USA) at an accelerating voltage of 20 kV to identify the surface functional groups and morphologies, respectively. The specific surface area, total pore volume and pore diameter were measured using the Brunauer, Emmett and Teller (BET) method (ASAP 2020, Micromeritics, USA). The crystalline structure was determined by X-Ray diffraction (XRD 6000, Shimadzu, Japan) using Cu Kα1 (λ= 1.5046 Å) with a X-Ray source through the 2θ range from 4° to 80°.Thermogravimetric analysis (TGA Labsys evo1150, Setaram, France) was carried out to determine the thermal stability.

The zero charge point is the pH at which the AC surface becomes neutral. This value (pH PZC) was determined using the following procedure: 50 ml of NaCl solution (0.01 M) with pH values ranging from 1 to 10 were prepared by adding NaOH solution 0.2 M and HCl solution 0.2 M. 100 mg of AC was added to each solution and left to stir for 48 hours at room temperature. The final pH after 48 hours was recorded to calculate the pH change. The pH PZC point was identified at the intersection of the curve (final pH - initial pH) and the straight line (final pH = initial pH), using a graphical representation of the data.

2.4. Batch Adsorption Studies

A stock solution was prepared at 0.1g.L^{-1} from AO7 as purchased. The concentrations required for the adsorption experiments were obtained by dilution with deionized water. The desired amount of AC, depending on the experimental conditions chosen, was added to the 100 ml dye solution under magnetic stirring (500 rpm) at room temperature (about 25°C). pH was 7.5 and remained unchanged during the adsorption experiments.. Once the adsorption process was complete, the solution mixture was passed through a 0.45 µm syringe filter. The filtrate obtained was then analyzed using a UV-visible spectrophotometer at a wavelength of 483 nm to determine the percentage of dye removal according to a calibration curve. The dye adsorption capacity and removal efficiency of the adsorbent were quantified using Equations (1) and (2), respectively.

$$q_t = \frac{C_0 - C_t}{M} * V \tag{1}$$

$$\%R = \frac{C_0 - C_t}{C_0} * 100 \tag{2}$$

where q_t (mg.g^{-1}) is the adsorption capacity at time t, R the AO7 dye removal efficiency, C_o the initial dye concentration, C_t (mg.L^{-1}) the dye concentration at time t, V (mL) the solution volume and M (g). the mass of the AC adsorbent

2.5. Adsorption Kinetics

Kinetics of the adsorption process were evaluated by varying the contact time between AO7 and AC. The experiment was carried out in a 200 ml suspension with a dye concentration of 30 mg.L^{-1} and 0.6 g AC. The concentration of dye in the solution was determined every 10 min until equilibrium was reached, when its value remained constant. The data were then fitted to pseudo-first-order and pseudo-second-order models (equations presented in Table 2).

Table 2. Kinetic models.

Kinetic Model	Equation	
Pseudo—first order	$\log(q_e - q_t) = \log q_e - \dfrac{K_f \times t}{2{,}303}$	(3)
Pseudo—second order	$\dfrac{t}{q_t} = \dfrac{1}{K_s \times q_e^2} + \dfrac{t}{q_e}$	(4)

where q_t and q_e (mg.g^{-1}) are the adsorption capacity at time t and equilibrium, respectively,and K_f and K_s are the pseudo-first-order (min^{-1}) and pseudo- second-order (g.(mg.min)$^{-1}$) adsorption rate constants, respectively.

2.6. Adsorption Isotherms

Adsorption isotherm models can be used to highlight the interactions of AO7 molecules with adsorption sites on the AC surface. This experiment examined the correlation between the amount of dye adsorbed at equilibrium and the amount of sorbent used. For this study, dye concentrations ranged from 10 to 90 mg.L^{-1}, while AC quantity and contact time were kept constant and equal to 0.3 g.L^{-1} and 60 min, respectively. Data adequacy and characterization of adsorbent surfaces as heterogeneous or homogeneous were assessed using Langmuir and Freundlich isotherm models (linearized equations presented in Table 3).

Table 3. Isotherm models.

Isotherm Model	Equation	
Langmuir	$q_e = \dfrac{1}{q_{max} \times \dfrac{1}{K_L \times q_{max} \times \dfrac{1}{C_e}}}$	(5)
Freundlich	$\log q_e = \log K_F + \dfrac{1}{n} \times \log C_e$	(6)

where q_{max} and qe (mg.g^{-1}) are the maximum monolayer adsorption capacity of the adsorbent and at equilibrium in Equations (5) and (6), respectively, C_e (mg.L^{-1}) the equilibrium value of the initial concentration, K_L the Langmuir constant, (mg.L^{-1} and K_F the Freundlich constant.

2.7. Adsorption Thermodynamics

Equilibrium adsorption isotherms were performed at three different temperatures (298, 321, and 339 K) to determine thermodynamic parameters, such as enthalpy, entropy, and Gibbs free energy, using equations 7-9 presented in Table 4.

Table 4. Thermodynamic parameters.

Thermodynamic parameters	Equation	
Gibbs free energy	$Kc = KL * 1000 * 55.51 * Mw$	(7)
	$\Delta G° = - RT \ln Kc$	(8)
Enthalpy Entropy	$\ln K_c = (\dfrac{\Delta S°}{R}) - (\dfrac{\Delta H°}{R}) * \dfrac{1}{T}$	(9)

where K_c (dimensionless) is the equilibrium constant; K_L (L.mg^{-1}) the Langmuir constant; *Mw* (g.mol^{-1}) the molecular weight of dye; T (°K) is the absolute temperature, R the ideal gas constant (8.314 J.mol^{-1}. K^{-1}); ΔG°(kJ.mol^{-1}) is the Gibbs free energy change; ΔH°(kJ.mol^{-1}) is the enthalpy change, ΔS°(J.mol-1.K^{-1}) is the entropy change.

2.8. Optimization of AO7 Removal by AC Adsorption

A Box-Benken quadratic three-factor response RSM model was developed to determine the impact of three independent variables on AO7 dye removal: contact time (X_1), initial dye concentration (X_2) and adsorbent dose (X_3). This approach made it possible to optimize the response

doi:10.20944/preprints202405.0964.v1

variable (Y) as a function of the input variables, while reducing the amount of experimental work required for adsorption studies. Design-Expert v12 software (Stat-Ease, USA) was applied to analyze the data using the RSM approach. In this study, the box in which the selected parameters were varied was 10-60 min for contact time, 10-90 mg.L^{-1} for initial dye concentration and 0.1-0.4 g.L^{-1} for adsorbent dose. 15 experiments were designed to optimize the combination of input variables, with AO7 dye removal efficiency (%) used as the output response. To assess model fit, analysis of variance (ANOVA) was used. The results derived from the experimental design, structured in three levels, were fitted using a model designed to capture the desired response. A classical polynomial regression equation was used to express the predicted response (Y):

$$Y(\%) = \mathrm{a}_0 + \sum a_i X_i + \sum\sum a_{ij} X_i X_j + \sum a_{ii} X_i^2, \qquad i \neq j \qquad (10)$$

where the X_i is the input factors that can influence the response Y, n the number of variables, a_0 the constant intercept, a_i the linear and a_{ii} the quadratic coefficient (with (i= 1, 2… n), a_{ij} (i= 1, 2… n-1; j = 2, … n) the interaction coefficient between two input factors. The regression and RSM model were used to investigate the highest projected dye removal.

3. Results and Discussion

3.1. Characteristics of the Prepared Activated Carbon

3.1.1. Chemical Group Analysis

The raw SCG mixture and the AC produced were compared using the FTIR technique to highlight the change in characteristic functional groups during activation (Figure 1a,b). The following band assignments were made based on the data found in the literature [32–34]:

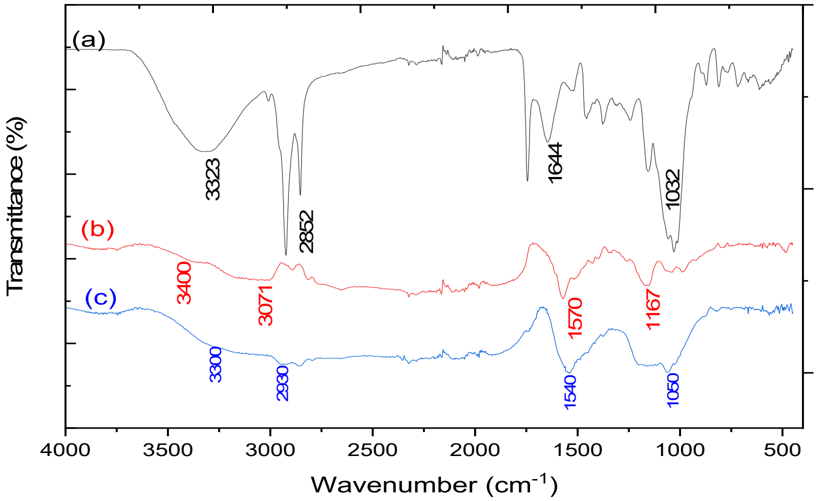

Figure 1. The FTIR spectrum for (a) SCG, (b) AC before and (c) after dye adsorption.

- The presence in the SCG spectrum (Figure 1a) of a broad transmission band between 3200-3600 cm^{-1} was attributed to the O-H stretching vibrations in cellulose, hemicellulose and lignin molecules. This band almost disappeared in the AC spectrum (Figure 1b) due to dehydration caused by the combination of H_3PO_4 and heat action.
- The sharp bands at 2800-3000 cm^{-1} can be assigned to stretch vibrations of the C-H bond in the saturated hydrocarbons. These strong absorptions in the SCG spectrum has been assumed to be due to the presence of components other than cellulose, hemicellulose and lignin molecules

[33]. These bands disappeared in the AC spectrum probably indicating their decomposition during pyrolysis.

- The bands between 1650-1750 cm^{-1} characteristic of carbonyl groups in the SCG spectrum revealed the presence of lignin and the strong absorption observed in the 1000-1200 cm^{-1} region linked to C-O stretching vibrations of cellulose, hemicellulose and lignin.
- As expected, AC showed stronger absorption than the starting CSG material in the 1600 cm^{-1} range corresponding the C=C vibrations in aromatic rings due to pyrolysis. On the other hand, the broad band around 1200 cm^{-1} was attributed to P=O and P-O-C vibrations associated with H_3PO_4 activation.

Comparison of AC spectra before and after dye adsorption (Figure 1b,c) revealed only slight changes due to a strong overlap of their respective characteristic bands. However, it can be observed an increase in absorption in the 1500-1550 cm^{-1} range linked to vibrations of azo groups (-N=N-), confirming the AO7 adsorption.

3.1.2. Structural Characterization

The X-ray diffraction was used to study the existence of crystalline structures and the amorphous nature within the AC matrix (Figure 2). The powder spectrum obtained revealed two diffraction peaks at about 2θ = 24 and 44° as is usually observed for AC prepared from different sources indicating that the activation process was successful [31,35–37]. The peaks observed are generally associated with the (002) and (100) reflection planes of graphite. However, as can be seen, the diffraction peaks are quite broad, suggesting that the structure of the prepared AC consisted of small crystalline phases dispersed in large disordered zones.

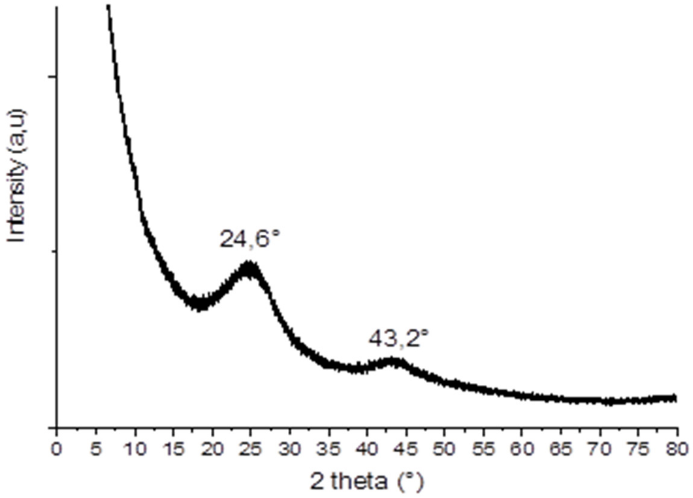

Figure 2. XRD pattern for the AC prepared from SCG.

The amorphous structure of adsorbent is expected to create a favorable microenvironment for adsorption of molecules in large quantities with stronger bond. In contrast, crystalline structures have uniform shapes, making the adsorption ability difficult. The AC prepared from SCG in this work presented a structure suitable for having good adsorption capability.

3.1.3. Morphological Analysis

SEM analysis provided useful information on the shape, size and structure of the AC powder particles (Figure 3). The irregular shaped particles showed a polydisperse size distribution, with dimensions ranging mainly from about 20 to 100 μm. In addition, SEM images enabled us to characterize the porous structure generated during the acid activation and pyrolysis processes. The outer surface of the particles had a macroporous morphology with cavity smaller than 20 µm. The enlargement in Figure 3 shows that interconnection by smaller pores in the cavities ensures the penetration and transfer of low-molecular-weight molecules from the surface to the inner microporosity of the adsorbent.

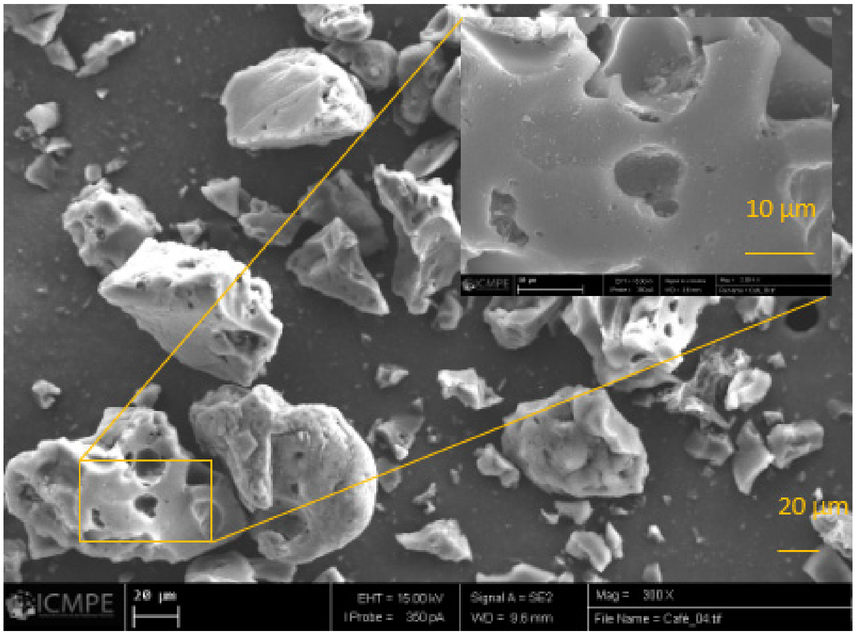

Figure 3. SEM surface image of AC prepared from SCG.

3.1.3. Textural Properties

Activated carbons are porous substances with a wide variety of pores ranging from macropores (> 50 nm), to mesopores (2-50 nm), and occasionally a small number of micropores (< 2 nm) depending on the activation process [18]. Gas adsorption, in particular nitrogen adsorption at 77 K, is a commonly used method for studying the characteristics of porous activated carbons. Figure 4a,b show the hysteresis of the adsorption isotherm and the pore distribution deduced for the AC sample, respectively. The material mainly exhibited a mesoporous structure according to IUPAC standards (Figure 4a; Type IV isotherm) [38], with a surface area and pore volume at 295 K of 29.38 m²/g and 0.067 cm³/g, respectively (Table 5). These values are easily explained by the reduction in the surface area and total volume of AC pores due to pyrolysis, which leads to pore collapse in composite materials [39]. However, given the small molecular size of the dyes, and of AO7 in particular (Table 1), the mean pore size (D_m) of 5.5 nm appears large enough to allow internal mass transfer of these compounds within the AC porous structure.

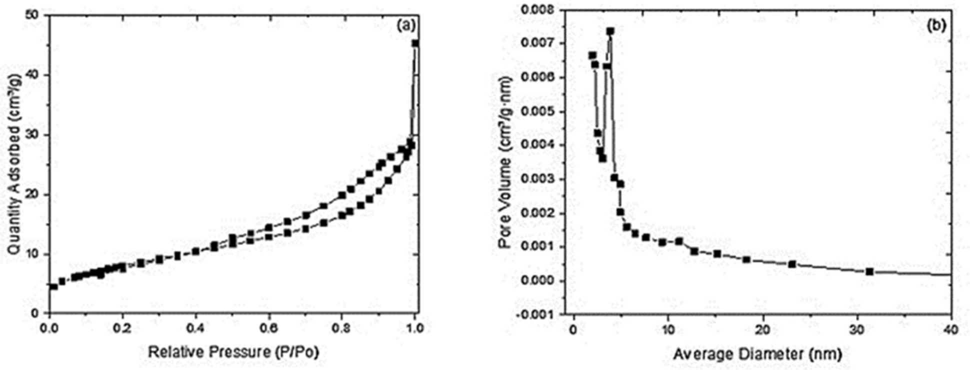

doi:10.20944/preprints202405.0964.v1

Figure 4. (a) N2 adsorption/desorption isotherms; (b) Pore size distribution of AC.

Table 5. BET measurements of AC.

	S_{BET} (m²/g)	V_{total} (cm³/g)	D_m (nm)
AC (from SCG)	29.38	0.067	5.5

3.1.5. Thermal Stability

Figure 5 shows the variation of AC weight between 50 and 1100°C using TGA. The thermogram obtained displays that a significant mass loss, equivalent to about 20%, occurred from 50°C to 150°C. It mainly corresponds to the removal of moisture (DTG peak at 100°C) and, possibly, of volatile compounds that accumulated within the porous structure of the material during its storage [40]. This result is indicative of the excellent adsorption properties of AC prepared in this work. Then, the curve shows a plateau up to 450°C with no significant mass loss revealing high thermal resistance and possible applications in this temperature range. After this second region, a gradual weight loss of about 30% is observed from 450°C to 1100°C. This mass decrease is due to decomposition of the oxygenated functions and partial degradation of the carbon skeleton [41,42].

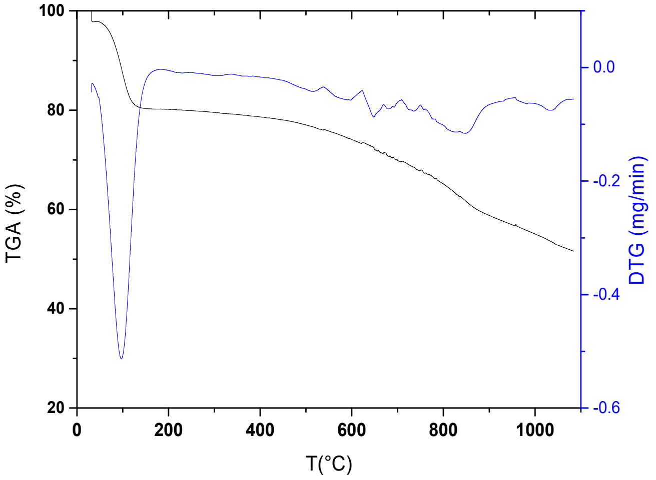

Figure 5. TGA and DTG curves of AC prepared from SCG.

3.1.6. pH Determination of Zero Charge Point

The surface charge of an adsorbent as a function of pH is an important parameter for the adsorption process, as it depends on the chemical groups present on the surface. Figure 6 presents the shift in pH AC suspension compared with the corresponding blank solutions. The intersection of curves at pH 2.4 indicates when the net AC surface charge becomes neutral at this value (pH PZC). This implies that for pH above this, the number of negatively charged surface functions is higher than that of positively charged functions, mainly due to deprotonation of carboxylic and phenolic groups [42].

doi:10.20944/preprints202405.0964.v1

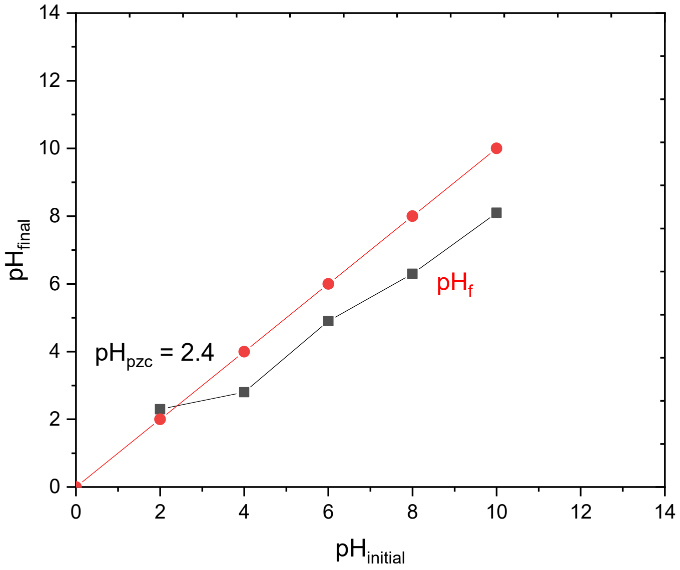

Figure 6. Determination of the point of zero charge pH.

3.2. Dye Adsorption Characterization

3.2.1. Adsorption Kinetics

Adsorption kinetics and analysis of the quantity adsorbed at equilibrium are the two key parameters for understanding and optimizing the adsorption process. The rate of removal of the AO7 dye from solution by AC was studied in order to establish the kinetic laws of adsorption. These experimental data were modeled using two theoretical approaches: the pseudo-first-order (PFO) model and the pseudo-second-order (PSO) model (Table 2). The best fitting for each of the two Equations 3 and 4 were obtained using the coefficients listed in Table 6. It was found that experimental data fitted much better the PSO model than the PFO model. The quantities of dye adsorbed on AC (qexp) were almost identical to those calculated (R^2 values close to unity). These results confirm the relevance of the PSO model to describe the adsorption kinetics of the AO7 dye on the AC surface and agree fully with previously reported data for the adsorption of various dyes on activated carbon [18].

Table 6. Kinetic parameters for AO7 adsorption.

Pseudo – first order			**Pseudo – second order**		
K_f (min^{-1})	q_e (mg.g^{-1})	R^2	K_s (mg.(g.min)$^{-1}$)	q_e (mg.g^{-1})	R^2
0.12	46.99	0.898	0.003	55.5	0.999

3.1.2. Adsorption Isotherms

Isotherm adsorption modeling makes it possible to determine the various equilibrium parameters, understand the degree of affinity, and interpret interaction mechanisms between adsorbent and adsorbate. Numerous models have been developed in the literature, taking into account parameters such as the number of layers of adsorbed molecules, surface heterogeneity and binding energies [18]. Langmuir and Freundlich isotherm models are the most frequently used due to their simplicity and consistency. The adsorption mechanism of AO7 by AC was analyzed using these two models. The optimized parameter values obtained for Equations 5 and 6 are listed in Table 7.

Table 7. Isotherm modeling parameters for AO7 adsorption.

Langmuir				**Freundlich**		
K_L (L.mol^{-1})	q_{max} (mg.g^{-1})	R^2	R_L	K_F (L.g^{-1})(L.mg^{-1})$^{1/n}$	1/n	R^2
0.38	129.87	0.9877	0.08	69.68	0.16	0.9733

The experimental results fit better with the Langmuir model based on homogeneous monolayer sorption ($R^2 = 0.9877$) than with the Freundlich model based on heterogeneous multilayer sorption. As a result, AO7 molecules are assumed to disperse in monolayers on adsorption sites that are identical in terms of energy and without electrostatic interactions between them [8]. The parameter RL is a measure of the separation factor between the adsorbate and adsorbent in a system. A value between 0 and 1 indicates a favorable adsorption process, while RL > 1 represents unfavorable adsorption. When RL = 1, adsorption is linear, and when its value is zero, the adsorption process is irreversible. The separation constant obtained by modeling in Table 6 (RL = 0.08<< 1) suggests a very strong but still reversible adsorption of AO7 by the AC prepared in this work.

3.1.3. Adsorption Thermodynamics

Thermodynamic factors, including standard free energy (ΔG°), enthalpy (ΔH°), and entropy (ΔS°), are key parameters in understanding the adsorption reaction. It is then possible to gain a deeper insight by identifying the spontaneity, heat exchange and degree of disorder of the process. Table 8 presents the values obtained in the temperature range 298-339°K using Equations (7)–(9).

Table 8. Thermodynamic parameters for AO7 adsorption on AC.

Thermodynamic parameters		**ΔG° (kJ.mol^{-1})**		**ΔH° (kJ.mol^{-1})**	**ΔS° (J.(mol.K)$^{-1}$)**
T (°K)	298	321	339		
	-7.43	-9.17	-10.53	15.12	75.65

The results led to the following conclusions:

The negative ΔG° values indicate that the adsorption process is favorable and spontaneous within the selected temperature range. The ΔG° values become more negative with increasing temperature, suggesting that the adsorption process is facilitated. This effect could be due to the widening of the AC pores with increasing temperature, resulting in easier diffusion of AO7 molecules and greater accessibility to adsorption sites located within the AC [41,43].

The positive ΔS° value indicates that the adsorption process is characterized by increased disorder in the interaction between AO7 dye molecules on the AC surface, confirming the favorable nature of adsorption.

The positive ΔH° value indicates that the dye adsorption process is endothermic in nature. Based on the ΔH° values, it can be deduced that adsorption is predominantly physisorption, through interactions between AO7 molecules and AC active sites such as hydrogen bonds and π-π interactions. This is confirmed by the fact that the ΔH° value is less than 40 kJ.mol−1 [44,45].

3.3. Adsorption Mechanism

Previous studies have shown that dye adsorption on activated carbon is influenced by various factors, such as electrostatic attraction, hydrogen bonding, Van der Waals interactions and π-π interactions. Interestingly, adsorption of the anionic dye occurs at pH values higher than the pH PZC of AC, while its surface charge is on average negative. Under these operating conditions, the predominant electrical interactions are repulsive, making adsorption unfavorable or limited even if a number of positive charges are present. This means that electrostatic interactions cannot be the main mechanism of AO7 adsorption and suggests the involvement of other types of interactions [8]. One possible mechanism is hydrogen bonding, as shown by the analysis of FTIR spectra (Figure 1). The characteristic peak for hydroxyl groups shows a red shift (move from 3400 cm^{-1} to 3300 cm^{-1}) and broadening after AO7 adsorption, pointing to hydrogen bonding between the hydroxyl groups on the AC surface and AO7. In addition, π-π interactions between the adsorbents and dye molecules seem to play a crucial role in the AO7 adsorption process. This is also supported by the FTIR analysis, which reveals a weakening of absorption intensity and a broadening of the characteristic C=C peak (1600 cm^{-1}) in the AC spectrum after AO7 adsorption (Figure 1), suggesting an interaction between the π-electron system of the AC structure and the aromatic rings of the AO7 dye molecules (Table 1) [44,45]. This is in perfect agreement with the endothermic nature of adsorption and the ΔH° value marking a physisorption mechanism and π-π type interactions, as mentioned above. Figure 7 presents the proposed interaction mechanisms occurring during the AO7 adsorption on AC prepared from SCG in this work.

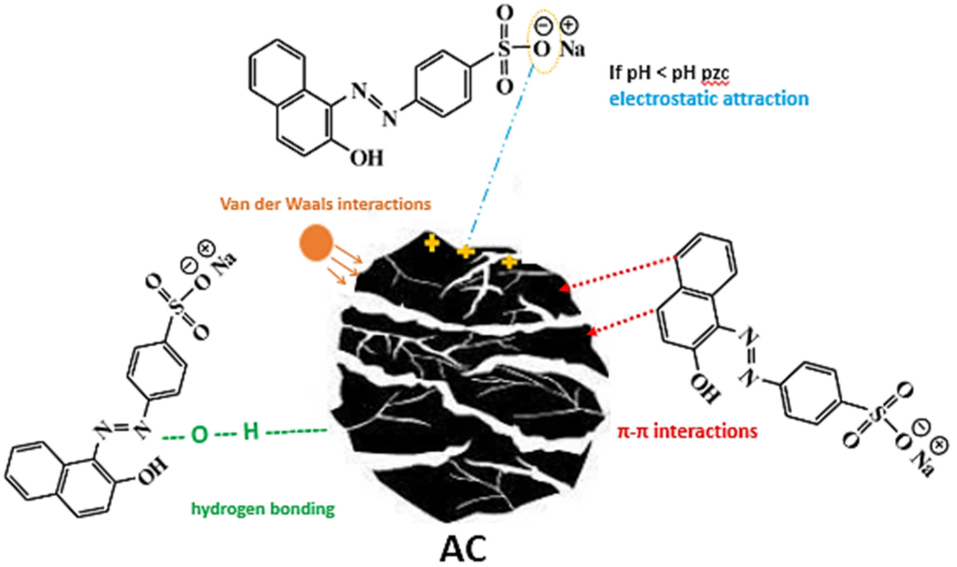

Figure 7. Proposed adsorption mechanisms of AO7 dye onto the activated carbon (AC).

3.4. Experimental Design and Response Surface Plots of AO7 Removal

Preliminary experiments showed that contact time, dye concentration and adsorbent dose were the key factors to be optimized. Although pH and temperature also had an influence, they were not of primary importance for the adsorption of AO7 on the AC prepared in this work. Therefore, to save time, these two parameters were kept at 7.5 and about 25°C while only the first three parameters mentioned were varied.

3.4.1. Statistical Analysis of the Derived Response Surface Model

In order to determine the optimum experimental conditions for AO7 removal efficiency by AC (output variable response) and to elucidate the weight of the different input parameters (X_1: contact time; X_2: dye concentration; X_3: adsorbent dose), batch adsorption experiments were carried out using the Box-Behnken design method as part of the RSM model. A series of 15 experiments was conducted according to a customized design, and the experimental and model-predicted responses are summarized in Table 9. The last column shows the residual calculated as the difference between the experimental responses and those predicted by the model. Depending on the value of the input factors, the percentage of dye removal varies between 15 and 98% with residual values well below 4%.

Table 9. Box–Behnken design and comparison of experimental and model-predicted results for AO7 adsorption using AC.

Test number	Factors			Response Y		Residual (% removal)
	X_1 (min)	X_2 (mg.L^{-1})	X_3 (g.L^{-1})	Experimental (% removal)	Predicted (% removal)	
1	60 (+1)	50 (+0)	0.100 (-1)	49.3	47.15	2.15
2	35 (+0)	50 (+0)	0.250 (+0)	84.0	85.45	-1.45
3	60 (+1)	10 (-1)	0.250 (+0)	97.2	97.19	0.0063
4	10 (-1)	90 (+1)	0.250 (+0)	47.0	45.55	1.45
5	35 (+0)	50 (+0)	0.250 (+0)	84.0	85.44	-1.44
6	10 (-1)	50 (+0)	0.100 (-1)	36.3	34.09	2.21
7	60 (+1)	90 (+1)	0.250 (+0)	51.0	49.56	1.44
8	35 (+0)	90 (+1)	0.400 (+1)	54.7	56.87	-2.17
9	10 (-1)	10 (-1)	0.250 (+0)	77.7	78.02	-0.3233
10	60 (+1)	50 (+0)	0.400 (+1)	98.0	94.39	3.61
11	35 (+0)	10 (-1)	0.100 (-1)	67.0	67.01	-0.0063
12	35 (+0)	10 (-1)	0.400 (+1)	98.0	100.16	-2.16
13	35 (+0)	50 (+0)	0.250 (+0)	81.1	78.02	3.1
14	35 (+0)	90 (+1)	0.100 (-1)	15.0	18.61	-3.61
15	10 (-1)	50 (+0)	0.400 (+1)	75.3	78.02	-2.72

Table 10 presents the analysis of variance (ANOVA) of the regression parameters of the quadratic response surface models predicted for percent dye removal. The *F*-value of 66.94 and the adjusted regression coefficient above 99% indicate that the model equation is highly significant. Furthermore, there is only a small probability of 0.01% that this *F*-value is due to noise [41].

Table 10. Analysis of variance for adsorption of AO7 dye by AC.

Source	Sum of squares	Degree of freedom	Mean of squares	*F*-value	*p*-value		R^2	R^2_{adj}
Model	8485.68	9	942.85	66.94	0.0001	significant	0.9918	0.9770
Error	17.39	2	8.69					

This analysis also makes it possible to determine the weight of the input parameters and their interaction through the polynomial coefficients of the model (Table 11). It appears from the *F*-values that X_1, X_2, X_3, X_1X_3, X_2X_3, X_{12} and X_{32} are the most significant terms in the model. In addition, *p*-values greater than 0.100 indicate that X_1X_2 and X_2^2 do not significantly contribute to the removal efficiency of AO7. Consequently, the polynomial Equation 10 can simply be written as follows:

$$Y(\%) = 78.02 + 6.54\,X_1 - 26.49\,X_2 + 11.4\,X_3 + 7.75\;X_1X_3 + 12.8\;X_2X_3 - 10.63\;X_1^2 - 7.64\;X_3^2 \quad (11)$$

Table 11. Estimated polynomial coefficients for adsorption of AO7 dye by AC.

Coefficient	**Estimated coefficient**	***F*-value**	***p*-value**
a_0	78.02		
a_1	6.54	24.32	0.0044
a_2	-26.49	398.7	<0.0001
a_3	11.40	73.82	0.0004
a_1a_2	-0.813	0.188	0.6831
a_1a_3	7.75	17.04	0.0091
a_2a_3	12.80	46.53	0.001
a_1^2	-10.63	29.61	0.0028

a_2^2	-1.08	0.307	0.6031
a_3^2	-7.64	15.3	0.0113

For the purpose of process optimization, Equation 11 of the model shows the extent to which dye removal efficiency is affected by the various input factors considered through their linear and quadratic terms, as well as their mutual interactions. Negative coefficients indicate that the corresponding factors have a negative impact on the removal efficiency [21]. The factor (X_2) is the most influential parameter: the higher the dye concentration, the lower the removal efficiency (Y). Contact time (X_1) and adsorbent dose (X_3) have antagonistic effects.

As mentioned above, the regression coefficient R^2 obtained in this study was 0.9918, indicating that the developed customized model accounted for about 99 % of the variability observed in the experimental data. In addition, the adjusted regression coefficient R^2_{adj} was 0.9770, which implies that nearly 98 % of the variability given the number of variables and degrees of freedom can be explained by the model. Figure 8 compares actual values with predicted model-derived responses for AO7 removal, illustrating the fit between the optimization model and experimental data. The proximity of the data points to the diagonal line in the plot of actual vs predicted values indicates the suitability of the model developed. This means that the statistical model effectively captures the correlation among the three factors investigated in AO7 removal. It was concluded that Equation 11 model is highly predictive and appropriate to accurately represent the relationship between the variables considered [29].

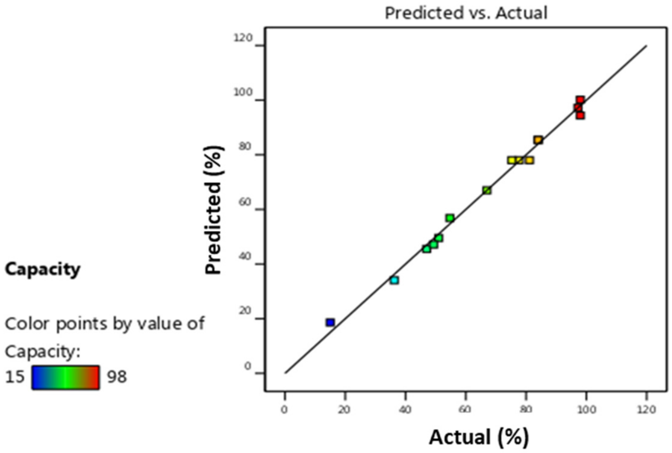

Figure 8. The removal efficiency predicted from Equation 11 (Y) versus the actual data (R) from Equation 2 for AO7 adsorption using AC.

3.4.2. Interaction Effect of Variables on Dye Removal Efficiency of AO7 Dye by AC

The 3D response surface plots and contour graphs for removal efficiency AO7 when using AC give a graphical interpretation of the second order model equation to examine the relationship between the different factors considered in the adsorption process.

1. **Dye concentration and adsorbent dosage**. Figure 9 illustrates the interaction effects of dye concentration and adsorbent dose on removal efficiency at a fixed time of 35 min. This shows that better responses were observed with higher adsorbent masses. This result shows the importance of the factors involving the input parameter X_3 in Equation 11. Increasing the amount of AC enhances the availability of active adsorption sites for dye binding, thus promoting the removal process [31]. On the other hand, increasing the dye concentration from 10 to 90 mg.L^{-1} while maintaining the AC dose at 0.250 g.L^{-1} results in a reduction in removal from 98% to 60%. The high removal efficiency of adsorbates at low concentrations can be attributed to the large number of adsorption sites available. This allows greater accessibility and

facilitated adsorption leading to the removal of a greater proportion of adsorbate from solution. It is important to note that the number of available sites is a major factor in determining the adsorption efficiency *Y*, showing the antagonistic impact of input parameters X_2 and X_3 in Equation 11. As the initial concentration of AO7 (X_2) increases, the number of available adsorption sites decreases, reducing the efficiency of adsorption removal [46].

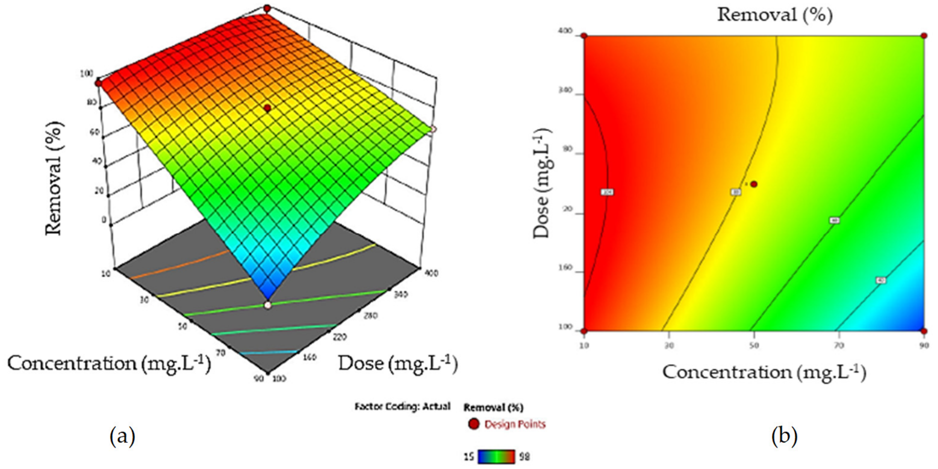

(a) (b)

Figure 9. (a) The response surface and (b) the contour map showing the interaction of AO7 concentration and AC dosage (input parameters X_2 and X_3 in Equation 11, respectively) on dye removal.

2. **Adsorbent dose and contact time.** The 3D response surface and contour map, illustrating the interaction effects of contact time (X_1) and adsorbent dose (X_3) on dye removal efficiency (*Y*) at a fixed dye concentration (50 mg.L^{-1}), are shown in Figure 10. It can be seen that for an AC adsorbent dose of less than 0.250 g.L^{-1}, contact time has a negligible effect on AO7 retention, as the available active sites are few in number and rapidly saturated. On the other hand, at a dose higher than 0.250 g.L^{-1}, AO7 retention increases with contact time up to 40 min, when retention becomes stable as all active sites are saturated and equilibrium is reached [47].

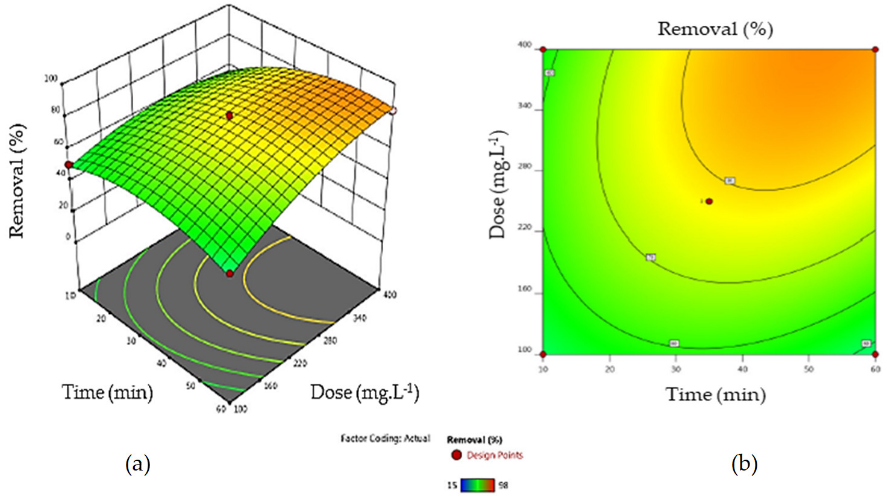

(a) (b)

Figure 10. (a) The response surface and (b) the contour map showing the interaction of contact time and AC dosage (input parameters X_1 and X_3 in Equation 11, respectively) on dye removal.

3. **Contact time and dye concentration**. The 3D graph and contour map shown in Figure 11 illustrate the combined influence of dye concentration (X_2) and contact time (X_1) on removal efficiency (*Y*). The experiment was carried out with a constant AC dosage of 0.250 mg.L^{-1}. The

doi:10.20944/preprints202405.0964.v1

contour map reveals an almost constant removal efficiency, indicating that AO7 adsorption remained relatively unchanged with varying contact time over the range studied. This lack of significant change in removal with contact time suggests rapid adsorption kinetics. However, increasing the dye concentration and maintaining a constant contact time leads to local saturation of the most easily accessible active sites. This phenomenon causes the driving force to remain at the same level until the adsorption process reaches equilibrium [48]. In general, the interaction of dye concentration and time of contact have a negative effect on the response variable.

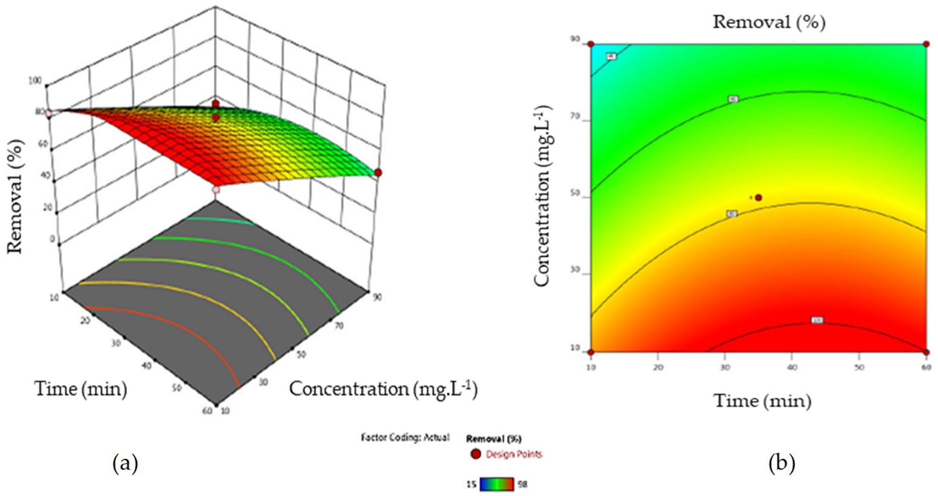

(a)

(b)

Figure 11. (a) The response surface and (b) the contour map showing the interaction of AO7 concentration and contact time (input parameters X_2 and X_1 in Equation 11, respectively).

3.4.3. Process Optimization

The optimum conditions in the range studied predicted by the model to ensure maximum AO7 removal were an adsorbent dose of 0.285 g.L^{-1}, for a dye concentration of 20 mg.L^{-1} and a contact time of 40 min. These conditions were expected to lead to a dye removal efficiency of 98%. An experiment was carried out using the specified parameters. The obtained results showed a discoloration rate of 97.6%, corresponding closely to the value predicted by the model. The agreement between experimental and predicted values confirms the accuracy and reliability of the customized model. Consequently, the model is considered a reliable tool for predicting and monitoring AO7 removal efficiency using AC.

3.4. Comparative Study

Table 12 compares the efficiency of the different adsorbents used to remove AO7 dye from aqueous solution reported in the literature [8,32,47,49–52]. As shown in this survey, the AC obtained from the SCG had excellent affinity for AO7 dye removal (in terms of adsorption capacity and kinetics) and compared favorably with the other low-cost activated carbon and bio-adsorbents. The dose of adsorbent required is comparatively low (0.285 g.L^{-1}) and the contact time is equally short (40 min), which may be explained by the high accessibility of adsorption sites, despite the low specific surface area (BET) of AC compared to activated carbon produced at higher temperatures. These operating conditions are very attractive and advantageous for a dye removal process using adsorption on activated carbon. Consequently, AC prepared from SCG according to the procedure described in this work is a promising adsorbent with great potential for the decolorization of wastewater from the textile industry.

Table 12. Comparative study of the adsorption of AO7 dye on various bio-sorbent from the literature.

Bio-sorbent	Experimental conditions				Results		Litt.
	pH	AO7 (mg.L^{-1})	Adsorbent dose (g.L^{-1})	Contact time (min)	Removal (%)	Capacity (mg.g^{-1})	
Bifurcaria bifurcate activated carbon	7.5	10	0.2	120	88.8	82.56	[8]
Activated carbon based on grape marc	2	150	2	180	-	140.5	[32]
Aloe vera leaves	2	50	2.5	360	-	15.9	[47]
Coconut coir activated carbon	3	40	6	120	99.5	13.16	[49]
Activated carbon from Pisum sativum pods	1.5	100	2	95.7	~100	473.93	[50]
Spent brewery grains	4.5	60	3.75	60	>90	30.5	[51]
Activated carbon from Casuarina wood	2.8	25	2	90	83.4	9.51	[52]
AC from SCG	7.5	20	0.285	40	98	119.51	[1]

[1] This study.

4. Conclusions

An activated carbon (AC) was successfully prepared from spent coffee grounds (SCG) by chemical activation with H_3PO_4 at the relatively low temperature of 600°C, making it a low-cost material. It was applied as an adsorbent to remove the azo dye AO7 from aqueous solution. Analysis of surface chemical functions by FTIR and a thermodynamic study revealed that AO7 adsorbs to AC by spontaneous physisorption involving mainly hydrogen bond and π-π interactions. Modeling of AO7 adsorption by AC showed that experimental kinetic and isotherm data fitted best with the pseudo-second-order model and the Langmuir model, respectively.

To optimize AO7 removal by AC, experimental design methodology was applied, allowing the influence of specific parameters such as contact time, dye concentration and adsorbent quantity to be determined. The optimal design model fitted with the experimental data showed a high coefficient of determination ($R^2 = 0.9918$) and an adjusted R^2 coefficient of 0.9770, indicating that it is a robust predictive model. In addition, the statistical significance was validated by a p-value associated with the model of less than 0.05. The optimal conditions for nearly complete removal of AO7 (98%) at a concentration of 20 mg.L^{-1}, predicted by the model and experimentally tested, required a contact time of 40 minutes and an adsorbent dosage of 0.285 g.L^{-1}.

Adsorption of dyes contained in textile industry wastewater using inexpensive, locally available activated carbon prepared from spent coffee grounds therefore appears to be a promising and effective treatment for pollution challenges, with strong potential for scale-up.

Author Contributions: Conceptualization, A.D. and R.B.A.; methodology, A.A. and L.D.; validation, A.D. and R.B.A.; investigation, F.A.; data curation, F.A., A.A. and L.D.; writing—original draft preparation, F.A., A.A. and R.B.A.; writing—review and editing, A.D.; supervision, A.D. and R.B.A. All authors have read and agreed to the published version of the manuscript.

Funding: This research received no external funding.

Institutional Review Board Statement: Not applicable.

Informed Consent Statement: Not applicable.

Acknowledgments: The authors gratefully acknowledge the characterization platform of Institut Européen des Membranes for analyses and F.A. the Research Unit "Advanced Technologies for Environment and Smart Cities", for her grant.

Data Availability Statement: The data presented in this study are available on request from the corresponding authors.

Conflicts of Interest: The authors declare no conflicts of interest.

References

1. Ahmed, J.; Thakur, A.; Goyal, A. Industrial Wastewater and Its Toxic Effects. In book Biological Treatment of Industrial Wastewater; Shah, M.P., Ed.; Publisher: The Royal Society of Chemistry, 2021, pp. 1-14. https://doi.org/10.1039/9781839165399-00001.
2. Ullah Khan, W.; Ahmed, S.; Dhoble, Y.; Madhav, S. A critical review of hazardous waste generation from textile industries and associated ecological impacts. *J. Indian Chem. Soc.* **2023**, *100*, 100829. https://doi.org/10.1016/j.jics.2022.100829.
3. Panhwar, A.; Jatoi, S.A.; Mazari, S.A.; Kandhro, A.; Rashid, U.; Qaisar, S. Water resources contamination and health hazards by textile industry effluent and glance at treatment techniques: A review. *Waste Management Bull*. **2024**, *1*, 158-163. https://doi.org/10.1016/j.wmb.2023.09.002.
4. Berradi, M.; Hsissou, R.; Khudhair, M.; Assouag, M.; Cherkaoui, O.; El Bachiri, A.; El Harfi, A. Textile finishing dyes and their impact on aquatic environs. *Heliyon* **2019**, *5*, e02711. 10.1016/j.heliyon.2019.e02711.
5. Perez-Calderon, J.; Marin-Silva, D.A.; Zaritzky, N.; Pinotti, A. Eco-friendly PVA-chitosan adsorbent films for the removal of azo dye Acid Orange 7: Physical cross-linking, adsorption process, and reuse of the material. *Adv. Ind. Eng. Polym. Res*. **2023**, *6*, 239-54. https://doi.org/10.1016/j.aiepr.2022.12.001.
6. Nistor, M.-A.; Halip L.; Muntean, S.G.; Kurunczi, L.; Costișor, O. Modeling and optimization of Acid Orange 7 adsorption process using magnetite/carbon nanocomposite. *Sustainable Chem. Pharm*. **2022**, *29*, 100778. https://doi.org/10.1016/j.scp.2022.100778.
7. Zhang, L.; Cheng, Z.; Guo, X.; Jiang, X.; Liu, R. Process optimization, kinetics and equilibrium of orange G and acid orange 7 adsorptions onto chitosan/surfactant. *J. Mol. Liq*. **2014,** *197*, 353-67. https://doi.org/10.1016/j.molliq.2014.06.007.
8. Bouzikri, S.; Ouasfi, N.; Khamliche. L. Bifurcaria bifurcata activated carbon for the adsorption enhancement of Acid Orange 7 and Basic Red 5 dyes: Kinetics, equilibrium and thermodynamics investigations. *Energy Nexus* **2022**, *7*, 100138. https://doi.org/10.1016/j.nexus.2022.100138.
9. Bouhaik, I.S.; Meliani, M.H.; Suleiman, R.K.; Saleh, T.A. Mechanistic insights into acid orange 7 azo dye (AO7) reduction using DFT calculations. *Polyhedron* **2023**, *245*, 116648. https://doi.org/10.1016/j.poly.2023.116648.
10. Ye, Q.; Wu, H.; Li, J.; Huang, Y.; Zhang, M. ; Yi, Q. ; Yan, B. Preparation of 1,8-dichloroanthraquinone/graphene oxide/poly (vinylidene fluoride) (1,8-AQ/GO/PVDF) mediator membrane and its application to catalyzing biodegradation of azo dyes. *Ecotoxicol. Env. Saf.* **2023**, *268*, 115681. https://doi.org/10.1016/j.ecoenv.2023.115681.
11. Shindhal, T.; Rakholiya, P.; Varjani, S.; Pandey, A.; Ngo, H.H.; Guo, W.; Ng, H. Y.; Taherzadeh, M.J. A critical review on advances in the practices and perspectives for the treatment of dye industry wastewater, *Bioengineered* **2021**, *12*, 70-87. https://doi.org/10.1080/21655979.2020.1863034.
12. Bai, X.; Sun, H.; Sun, J.; Zhu, Z. Efficient removal of sixteen priority polycyclic aromatic hydrocarbons from textile dyeing sludge using electrochemical Fe2+-activated peroxymonosulfate oxidation - A green pretreatment strategy for textile dyeing sludge toxicity reduction. *J. Hazard. Mater*. **2022**, *435*, 129087. https://doi.org/10.1016/j.jhazmat.2022.129087.
13. Ihaddaden, S.; Aberkane, D. ; Boukerroui, A.; Robert, D. Removal of methylene blue (basic dye) by coagulation-flocculation with biomaterials (bentonite and Opuntia ficus indica). *J. Water Process Eng.* **2022**, *49*, 102952. https://doi.org/10.1016/j.jwpe.2022.102952.
14. Khmiri, Y.; Attia, A.; Aloulou, H.; Dammak, L.; Baklouti, L.; Ben Amar R. Preparation and Characterization of New and Low-Cost Ceramic Flat Membranes Based on Zeolite-Clay for the Removal of Indigo Blue Dye Molecules. *Membranes* **2023**, *13*, 865. https://doi.org/10.3390/membranes13110865.
15. Benkhaya, S.; M'rabet, S.; Hsissou, R.; El Harfi, A. Synthesis of new low-cost organic ultrafiltration membrane made from Polysulfone/Polyetherimide blends and its application for soluble azoic dyes removal. *J Mater. Res. Technol*. **2020**, *9*, 4763-72. https://doi.org/10.1016/j.jmrt.2020.02.102.
16. Sun, C.; Liu, H. Room temperature route to silsesquioxane-based porphyrin functional NIR porous polymer for efficient photodegradation of azo-dyes under sunlight. *Next Materials* **2024**, *2*, 100123. https://doi.org/10.1016/j.nxmate.2024.100123.

17. Samadi, A.; Wang, Z.; Wang, Shaobin; Nataraj, S.K.; Kong, L.; Zhao, S. Polyaniline-based adsorbents for water treatment: Roles of low-cost materials and 2D materials. *Chem. Eng. J.* **2023**, *478*, 147506. https://doi.org/10.1016/j.cej.2023.147506.
18. Husien, S.; El-taweel, R.M.; Salim, A.I.; Fahim, I.S.; Said, L.A.; Radwan, A.G. Review of activated carbon adsorbent material for textile dyes removal: Preparation, and modelling. *Curr. Res. Green Sustainable Chem.* **2022**, *5*, 100325. https://doi.org/10.1016/j.crgsc.2022.100325.
19. Gayathiri, M.; Pulingam, T.; Lee, K.T.; Sudesh, K. Activated carbon from biomass waste precursors: Factors affecting production and adsorption mechanism, *Chemosphere*, **2022**, *294*, 133764. https://doi.org/10.1016/j.chemosphere.2022.133764.
20. Jung, K.-W.; Choi, B.H.; Hwang, M.-J.; Jeong, T.-U.; Ahn, K.-H. Fabrication of granular activated carbons derived from spent coffee grounds by entrapment in calcium alginate beads for adsorption of acid orange 7 and methylene blue. *Bioresour. Technol*. **2016**, *219*, 185-95. https://doi.org/10.1016/j.biortech.2016.07.098.
21. Azzouni, D.; Baragh, F.; Mahmoud, A. M.; Alanazi, M. M.; Rais, Z.; Taleb, M. Optimization of methylene blue removal from aqueous solutions using activated carbon derived from coffee ground pyrolysis: A response surface methodology (RSM) approach for natural and cost-effective adsorption. *J. Saudi Chem. Soc*. **2023**, *27*, 101695. https://doi.org/10.1016/j.jscs.2023.101695.
22. Kłosek-Wawrzyn, E.; Frąc, M.; Pichór, W. Influence of pregranulation and low-pressure compaction on the properties of ceramic materials incorporating clay and spent coffee grounds. *Appl. Clay Sci*. **2023**, *245*, 107154. https://doi.org/10.1016/j.clay.2023.107154.
23. McNutt, J.; He, Q. (Sophia). Spent Coffee Grounds: A Review on Current Utilization. *J. Ind. Eng. Chem*. **2019**, *71*, 78–88. https://doi.org/10.1016/j.jiec.2018.11.054.
24. Ma, W.; Fan, J.; Cui, X.; Wang, Y.; Yan, Y.; Meng, Z.; Gao, H.; Lu, R.; Zhou, W. Pyrolyzing Spent Coffee Ground to Biochar Treated with H3PO4 for the Efficient Removal of 2,4-Dichlorophenoxyacetic Acid Herbicide: Adsorptive Behaviors and Mechanism. *J. Environ. Chem. Eng*. **2023**, *11*, 109165. https://doi.org/10.1016/j.jece.2022.109165.
25. Obar, F.; Pradhan, S.; Mackey, H. R.; McKay, G. Removal of Lithium from Aqueous Solution by Spent Coffee Ground Activated Biochar. *Process Saf. Environ. Prot*. **2024**, *184*, 680–689. https://doi.org/10.1016/j.psep.2024.02.020.
26. Bose, S.; Kirk, R. D.; Maslen, H.; Pardo Islas, M. A.; Smith, B.; Dugmore, T. I. J.; Matharu, A. S. Mesoporous-Rich Calcium and Potassium-Activated Carbons Prepared from Degreased Spent Coffee Grounds for Efficient Removal of MnO42− in Aqueous media. *RSC Adv*. **2022**, *12*, 19417–19423. https://doi.org/10.1039/d2ra02214a.
27. Sani, M. N. H.; Amin, M.; Siddique, A. B.; Nasif, S. O.; Ghaley, B. B.; Ge, L.; Wang, F.; Yong, J. W. H. Waste-Derived Nanobiochar: A New Avenue towards Sustainable Agriculture, Environment, and Circular Bioeconomy. *Sci. Total Environ*. **2023**, *905*, 166881. https://doi.org/10.1016/j.scitotenv.2023.166881.
28. Solihat, N. N.; Hidayat, A. F.; Ilyas, R. A.; Thiagamani, S. M. K.; Azeele, N. I. W.; Sari, F. P.; Ismayati, M.; Bakshi, M. I.; Garba, Z. N.; Hussin, M. H.; Restu, W. K.; Syafii, W.; Ariyanta, H. A.; Fatriasari, W. Recent Antibacterial Agents from Biomass Derivatives: Characteristics and Applications. *J. Bioresour. Bioprod*. **2024**, in press. https://doi.org/10.1016/j.jobab.2024.02.002.
29. Babakhani, A.; Sartaj, M. Optimization of Nickel(II) Adsorption by Sodium Tripolyphosphate Crosslinked Chitosan Using Response Surface Methodology (RSM). *Sustain. Chem. Environ*. **2023**, *2*, 100019. https://doi.org/10.1016/j.scenv.2023.100019.
30. Ahmad, A.; Yadav, A. K. Parametric Analysis of Wastewater Electrolysis for Green Hydrogen Production: A Combined RSM, Genetic Algorithm, and Particle Swarm Optimization Approach. *Int. J. Hydrog. Energy* **2024**, *59*, 51–62. https://doi.org/10.1016/j.ijhydene.2024.01.302.
31. Nure, J. F.; Mengistu, A.; Abewaa, M.; Angassa, K.; Moyo, W.; Phiri, Z.; Mafa, P. J.; Kuvarega, A. T.; Nkambule, T. T. I. Adsorption of Black MNN Reactive Dye from Tannery Wastewater Using Activated Carbon of Rumex Abysinicus. *J. Taiwan Inst. Chem. Eng.* **2023**, *151*, 105138. https://doi.org/10.1016/j.jtice.2023.105138.
32. Al, K. and Başakçılardan Kabakcı, S. Oxygen-Rich Precursors via Glycerol Organosolv Treatment: Preparation of Activated Carbon from Hazelnut Shell and Its Structural Components for Possible Use in Electrodes for Supercapacitors. *Int. J. Thermofluids* **2024**, *21*, 100588. https://doi.org/10.1016/j.ijft.2024.100588.
33. Chavhan, M. P.; Slovák, V.; Siddiqi, H.; Mucha, M. Pyrolysis of Household Coffee Vis-à-Vis Tea Waste: A Detailed Insight into Physicochemical Properties, Kinetics, and Thermodynamics Study. *Chem. Eng. J. Adv.* **2024**, *17*, 100587. https://doi.org/10.1016/j.ceja.2024.100587.
34. Bourahla, S.; Nemchi, F.; Belayachi, H.; Belayachi, A.; Harrats, C.; Belhakem, M. Removal of the AO7 Dye by Adsorption on Activated Carbon Based on Grape Marc: Equilibrium, Regeneration, and FTIR Spectroscopy. *J. Iran. Chem. Soc.* **2023**, *20*, 669–681. https://doi.org/10.1007/s13738-022-02705-6.
35. Dhelipan, M.; Arunchander, A.; Sahu, A.K.; Kalpana, D. Activated carbon from orange peels as supercapacitor electrode and catalyst support for oxygen reduction reaction in proton exchange membrane fuel cell. *J. Saudi Chem. Soc*. **2017**, *21*, 487–494. http://dx.doi.org/10.1016/j.jscs.2016.12.003.

36. Keppetipola, N.; Maithri, M.; Dissanayake, P.; Karunarathne, B.; Dourges, M.A.; Talaga, D.; Servant, L.; Olivier, C.; Toupance, T.; Uchida, S.; Tennakone, K.; Kumara G.R.A.; Cojocaru. L. Graphite-type activated carbon from coconut shell: a natural source for eco-friendly non-volatile storage devices. *RSC Adv*. **2021**, *11*, 2854-2865. https://doi.org/10.1039/D0RA09182K.
37. Lazzarini, A.; Piovano, A.; Pellegrini, R.; Agostini, G.; Rudiü, S.; Lambertia, C.; Groppo, E. Graphitization of activated carbons: a molecular-level investigation by INS, DRIFT, XRD and Raman techniques, *Physics Procedia* **2016**, *85*, 20–26 https://doi.org/10.1016/j.phpro.2016.11.076.
38. Jedynak, K.; Szczepanik, B.; R˛edzia, N.; Słomkiewicz, P.; Kolbus, A.; Rogala, P. Ordered mesoporous carbons for adsorption of paracetamol and non-steroidal anti-inflammatory drugs: Ibuprofen and naproxen from aqueous solutions. *Water* **2019**, *11*, 1099. https://doi.org/10.3390/w11051099.
39. Schütz, T.; Dolinská, S.; Hudec, P.; Mockovčiaková, A.; Znamenáčková, I. Cadmium adsorption on manganese modified bentonite and bentonite–quartz sand blend. *Int. J. Miner. Process*. **2016**, *150*, 32-38. https://doi.org/10.1016/j.minpro.2016.03.003.
40. Dziejarski, B.; Hernández-Barreto, D. F.; Moreno-Piraján, J. C.; Giraldo, L.; Serafin, J.; Knutsson, P.; Andersson, K.; Krzyżyńska, R. Upgrading Recovered Carbon Black (rCB) from Industrial-Scale End-of-Life Tires (ELTs) Pyrolysis to Activated Carbons: Material Characterization and CO2 Capture Abilities. *Environ. Res.* **2024**, *247*, 118169. https://doi.org/10.1016/j.envres.2024.118169.
41. Romdhani, M.; Attia, A.; Charcosset, C.; Mahouche-Chergui, S.; Ates, A.; Duplay, J.; Ben Amar, R. Optimization of Paracetamol and Chloramphenicol Removal by Novel Activated Carbon Derived from Sawdust Using Response Surface Methodology. *Sustainability* **2023**, *15*, 2516. https://doi.org/10.3390/su15032516.
42. Bernal, V.; Giraldo, L.; Moreno-Piraján, J.C. Physicochemical Properties of Activated Carbon: Their Effect on the Adsorption of Pharmaceutical Compounds and Adsorbate–Adsorbent Interactions. *C* **2018**, *4*, 62. https://doi.org:10.3390/c4040062.
43. Amellal, T.; Boukhalfa, N.; Meniai, A. H. Enhanced Removal of Basic Brown1 Dye from Aqueous Solutions by Sawdust Activated Carbon. Equilibrium, Thermodynamic and Kinetics. *Desalin. Water Treat.* **2024**, *317*, 100057. https://doi.org/10.1016/j.dwt.2024.100057.
44. Zhang, T.; Zhang, X.; Li, H. Kinetics and Equilibrium Study of Phenol Adsorption by Activated Carbon Derived from Pig Blood. *Carbon Trends* **2023**, *12*, 100281. https://doi.org/10.1016/j.cartre.2023.100281.
45. Cao, S.; Zhu, R.; Wu, D.; Su, H.; Liu, Z.; Chen, Z. How hydrogen bonding and π–π interactions synergistically facilitate mephedrone adsorption by bio-sorbent: An in-depth microscopic scale interpretation. *Environ. Pollut*. **2024**, *342*, 123044. https://doi.org/10.1016/j.envpol.2023.123044.
46. Khumalo, S. M.; Bakare, B. F.; Rathilal, S. Single and Multicomponent Adsorption of Amoxicillin, Ciprofloxacin, and Sulfamethoxazole on Chitosan-Carbon Nanotubes Hydrogel Beads from Aqueous Solutions: Kinetics, Isotherms, and Thermodynamic Parameters. *J. Hazard. Mater. Adv*. **2024**, *13*, 100404. https://doi.org/10.1016/j.hazadv.2024.100404.
47. Hisana; Shahzaib, A.; Nishat, N.; Alshehri, S. M.; Ahamad, T.; Haque, Z. Biogenically Fabricated Tulsi-Infused ZnO–CuO Nanocomposites for Enhanced Dye Reduction and Adsorption. *Hybrid Adv*. **2024**, *5*, 100145. https://doi.org/10.1016/j.hybadv.2024.100145.
48. Aguilar, M. I.; Lloréns, M.; Ortuño, J. F.; Meseguer, V. F.; Pérez-Marín, A. B.; Cases, A. Use of the Box–Behnken Experimental Design for the Optimization of Orange II (Acid Orange 7) Adsorption on Aloe Vera. *Sustainability* **2023**, *15*, 15727. https://doi.org/10.3390/su152215727.
49. Chaudhuri, M.; Zaid, N. A. M.; Elmolla, E. S. Coconut Coir Activated Carbon: An Adsorbent for Removal of Textile Acid Azo Dye from Aqueous Solution. In book 2012 IEEE Colloquium on Humanities, Science and Engineering (CHUSER); Publisher: IEEE, 2012, pp 58–62. https://doi.org/10.1109/CHUSER.2012.6504281.
50. El-Nemr, M. A.; El Nemr, A.; Hassaan, M. A.; Ragab, S.; Tedone, L.; De Mastro, G.; Pantaleo, A. Microporous Activated Carbon from Pisum Sativum Pods Using Various Activation Methods and Tested for Adsorption of Acid Orange 7 Dye from Water. *Molecules*, **2022**, *27*, 154840. https://doi.org/10.3390/molecules27154840.
51. Silva J.P., Sousa S., Rodrigues J., Antunes H., Porter J.J., Gonçalves I., Ferreira-Dias S. Adsorption of acid orange 7 dye in aqueous solutions by spent brewery grains. *Sep. Purif. Technol*. **2004**, *40*, 309-15. https://doi.org/10.1016/j.seppur.2004.03.010.
52. Supriya S., Palanisamy P.N. Adsorptive removal of acid orange 7 from industrial effluents using activated carbon and conducting polymer composite–A comparative study. *Indian J. Chem. Technol*. **2016**, *23*, 506-512. https:// doi: 10.56042/ijct.v23i6.5781.